

Identification of a CpG Island Methylator Phenotype that Defines a Distinct Subgroup of Glioma

Houtan Noushmehr,^{1,13} Daniel J. Weisenberger,^{1,13} Kristin Diefes,^{2,13} Heidi S. Phillips,³ Kanan Pujara,³ Benjamin P. Berman,¹ Fei Pan,¹ Christopher E. Pelloso,⁴ Erik P. Sulman,⁴ Krishna P. Bhat,² Roel G.W. Verhaak,^{5,6} Katherine A. Hoadley,^{7,8} D. Neil Hayes,^{7,8} Charles M. Perou,^{7,8} Heather K. Schmidt,⁹ Li Ding,⁹ Richard K. Wilson,⁹ David Van Den Berg,¹ Hui Shen,¹ Henrik Bengtsson,¹⁰ Pierre Neuvial,¹⁰ Leslie M. Cope,¹¹ Jonathan Buckley,^{1,12} James G. Herman,¹¹ Stephen B. Baylin,¹¹ Peter W. Laird,^{1,14,*} Kenneth Aldape,^{2,14} and The Cancer Genome Atlas Research Network

¹USC Epigenome Center, University of Southern California, Los Angeles, CA 90033, USA

²Department of Pathology, The University of Texas MD Anderson Cancer Center, Houston, TX 77030, USA

³Department of Tumor Biology and Angiogenesis, Genentech, Inc., South San Francisco, CA 94080, USA

⁴Department of Radiation Oncology, The University of Texas MD Anderson Cancer Center, Houston, TX 77030, USA

⁵The Eli and Edythe L. Broad Institute of Massachusetts Institute of Technology and Harvard University, Cambridge, MA 02142, USA

⁶Department of Medical Oncology, Dana-Farber Cancer Institute, Boston, MA 02115, USA

⁷Department of Genetics

⁸Lineberger Comprehensive Cancer Center

University of North Carolina at Chapel Hill, Chapel Hill, NC 27599, USA

⁹The Genome Center at Washington University, Department of Genetics, Washington University School of Medicine, St. Louis, MI 63108, USA

¹⁰Department of Statistics, University of California, Berkeley, CA 94720, USA

¹¹Department on Oncology, Johns Hopkins School of Medicine, Baltimore, MD 21231, USA

¹²Department of Preventive Medicine, Keck School of Medicine, University of Southern California, Los Angeles, CA 90033, USA

¹³These authors contributed equally to this work

¹⁴These authors contributed equally to this work

*Correspondence: plaird@usc.edu

DOI 10.1016/j.ccr.2010.03.017

SUMMARY

We have profiled promoter DNA methylation alterations in 272 glioblastoma tumors in the context of The Cancer Genome Atlas (TCGA). We found that a distinct subset of samples displays concerted hypermethylation at a large number of loci, indicating the existence of a glioma-CpG island methylator phenotype (G-CIMP). We validated G-CIMP in a set of non-TCGA glioblastomas and low-grade gliomas. G-CIMP tumors belong to the proneural subgroup, are more prevalent among lower-grade gliomas, display distinct copy-number alterations, and are tightly associated with *IDH1* somatic mutations. Patients with G-CIMP tumors are younger at the time of diagnosis and experience significantly improved outcome. These findings identify G-CIMP as a distinct subset of human gliomas on molecular and clinical grounds.

INTRODUCTION

Human gliomas present as heterogeneous disease, primarily defined by the histologic appearance of the tumor cells. Astrocytoma and oligodendroglioma constitute the infiltrating gliomas (Adamson et al., 2009). The cell or cells of origin have not defin-

itively been identified, however, the identification of tumorigenic, stem-cell like precursor cells in advanced stage gliomas suggests that human gliomas may have a neural stem cell origin (Canoll and Goldman, 2008; Dirks, 2006; Galli et al., 2004).

Gliomas are subdivided by the World Health Organization (WHO) by histological grade, which is an indication of

Significance

Glioblastoma (GBM) is a highly aggressive form of brain tumor, with a patient median survival of just over one year. The Cancer Genome Atlas (TCGA) project aims to characterize cancer genomes to identify means of improving cancer prevention, detection, and therapy. Using TCGA data, we identified a subset of GBM tumors with characteristic promoter DNA methylation alterations, referred to as a glioma CpG island methylator phenotype (G-CIMP). G-CIMP tumors have distinct molecular features, including a high frequency of *IDH1* mutation and characteristic copy-number alterations. Patients with G-CIMP tumors are younger at diagnosis and display improved survival times. The molecular alterations in G-CIMP tumors define a distinct subset of human gliomas with specific clinical features.

differentiation status, malignant potential, response to treatment, and survival. Glioblastoma (GBM), also described as grade IV glioma, accounts for more than 50% of all gliomas (Adamson et al., 2009). Patients with GBM have an overall median survival time of only 15 months (Brandes et al., 2001; Martinez et al., 2010; Parsons et al., 2008). Most GBMs are diagnosed as de novo or primary tumors and are more common in males. A subset of ~5% of GBM tumors, termed secondary GBM, progress from lower-grade tumors (grade II/III), are seen in younger patients, are more evenly distributed among the sexes, and exhibit longer survival times (reviewed in Adamson et al., 2009; Furnari et al., 2007).

There is currently great interest in characterizing and compiling the genome and transcriptome changes in human GBM tumors to identify aberrantly functioning molecular pathways and tumor subtypes. The Cancer Genome Atlas (TCGA) pilot project identified genetic changes of primary DNA sequence and copy number, DNA methylation, gene expression, and patient clinical information for a set of GBM tumors (The Cancer Genome Atlas Research Network, 2008). TCGA also reaffirmed genetic alterations in *TP53*, *PTEN*, *EGFR*, *RB1*, *NF1*, *ERBB2*, *PIK3R1*, and *PIK3CA* mutations and detected an increased frequency of *NF1* mutations in GBM patients (The Cancer Genome Atlas Research Network, 2008). Recent DNA sequencing analyses of primary GBM tumors with a more comprehensive approach (Parsons et al., 2008) also identified somatic mutations in isocitrate dehydrogenase 1 (*IDH1*) that occur in 12% of all GBM patients. *IDH1* mutations have only been detected at the arginine residue in codon 132, with the most common change being the R132H mutation (Parsons et al., 2008; Yan et al., 2009), which results in a gain of enzyme function in directly catalyzing α -ketoglutarate to *R*(-)-2-hydroxyglutarate (Dang et al., 2009). *IDH1* mutations are enriched in secondary GBM cases and younger individuals and are coincident with increased patient survival (Balss et al., 2008; Hartmann et al., 2009; Yan et al., 2009). Higher *IDH1* mutation rates are seen in grade II and III astrocytomas and oligodendrogliomas (Balss et al., 2008; Bleeker et al., 2009; Hartmann et al., 2009; Yan et al., 2009), suggesting that *IDH1* mutations generally occur in the progressive form of glioma, rather than in de novo GBM. Mutations in the related *IDH2* gene are of lower frequency and generally nonoverlapping with tumors containing *IDH1* mutations (Hartmann et al., 2009; Yan et al., 2009).

Cancer-specific DNA methylation changes are hallmarks of human cancers, in which global DNA hypomethylation is often seen concomitantly with hypermethylation of CpG islands (reviewed in Jones and Baylin, 2007). Promoter CpG island hypermethylation generally results in transcriptional silencing of the associated gene (Jones and Baylin, 2007). CpG island hypermethylation events have also been shown to serve as biomarkers in human cancers, for early detection in blood and other bodily fluids, for prognosis or prediction of response to therapy, and to monitor cancer recurrence (Laird, 2003).

A CpG island methylator phenotype (CIMP) was first characterized in human colorectal cancer by Toyota and colleagues (Toyota et al., 1999) as cancer-specific CpG island hypermethylation of a subset of genes in a subset of tumors. We confirmed and further characterized colorectal CIMP using MethyLight technology (Weisenberger et al., 2006). Colorectal CIMP is char-

acterized by tumors in the proximal colon, a tight association with *BRAF* mutations, and microsatellite instability caused by *MLH1* promoter hypermethylation and transcriptional silencing (Weisenberger et al., 2006).

DNA methylation alterations have been widely reported in human gliomas, and there have been several reports of promoter-associated CpG island hypermethylation in human GBM and other glioma subtypes (Kim et al., 2006; Martinez et al., 2009; Martinez et al., 2007; Nagarajan and Costello, 2009; Stone et al., 2004; Tepel et al., 2008; Uhlmann et al., 2003). Several studies have noted differences between primary and secondary GBMs with respect to epigenetic changes. Overall, secondary GBMs have a higher frequency of promoter methylation than primary GBM (Ohgaki and Kleihues, 2007). In particular, promoter methylation of *RB1* was found to be approximately three times more common in secondary GBM (Nakamura et al., 2001).

Hypermethylation of the *MGMT* promoter-associated CpG island has been shown in a large percentage of GBM patients (Esteller et al., 2000; Esteller et al., 1999; Hegi et al., 2005; Hegi et al., 2008; Herman and Baylin, 2003). *MGMT* encodes for an O6-methylguanine methyltransferase that removes alkyl groups from the O-6 position of guanine. GBM patients with *MGMT* hypermethylation showed sensitivity to alkylating agents such as temozolomide, with an accompanying improved outcome (Esteller et al., 2000; Esteller et al., 1999; Hegi et al., 2005; Hegi et al., 2008; Herman and Baylin, 2003). However, initial promoter methylation of *MGMT*, in conjunction with temozolomide treatment, may result in selective pressure to lose mismatch repair function, resulting in aggressive recurrent tumors with a hypermutator phenotype (Cahill et al., 2007; Hegi et al., 2005; Silber et al., 1999; The Cancer Genome Atlas Research Network, 2008).

Here, we report the DNA methylation analysis of 272 GBM tumors collected for TCGA, extend this to lower-grade tumors, and characterize a distinct subgroup of human gliomas exhibiting CIMP.

RESULTS

Identification of a Distinct DNA Methylation Subgroup within GBM Patients

We determined DNA methylation profiles in a discovery set of 272 TCGA GBM samples. At the start of this study, we relied on the Illumina GoldenGate platform, using both the standard Cancer Panel I, and a custom-designed array (The Cancer Genome Atlas Research Network, 2008) (Figures S1A–S1C available online and Experimental Procedures), but migrated to the more comprehensive Infinium platform (Figure 1 and Figure S1C), as it became available. DNA methylation measurements were highly correlated for CpG dinucleotides shared between the two platforms (Pearson's $r = 0.94$, Figure S1D). Both platforms interrogate a sampling of about two CpG dinucleotides per gene. Although this implies that nonrepresentative CpGs may be assessed for some promoters, it is likely that representative results will be obtained for most gene promoters, given the very high degree of locally correlated DNA methylation behavior (Eckhardt et al., 2006).

We selected the most variant probes on each platform and performed consensus clustering to identify GBM subgroups

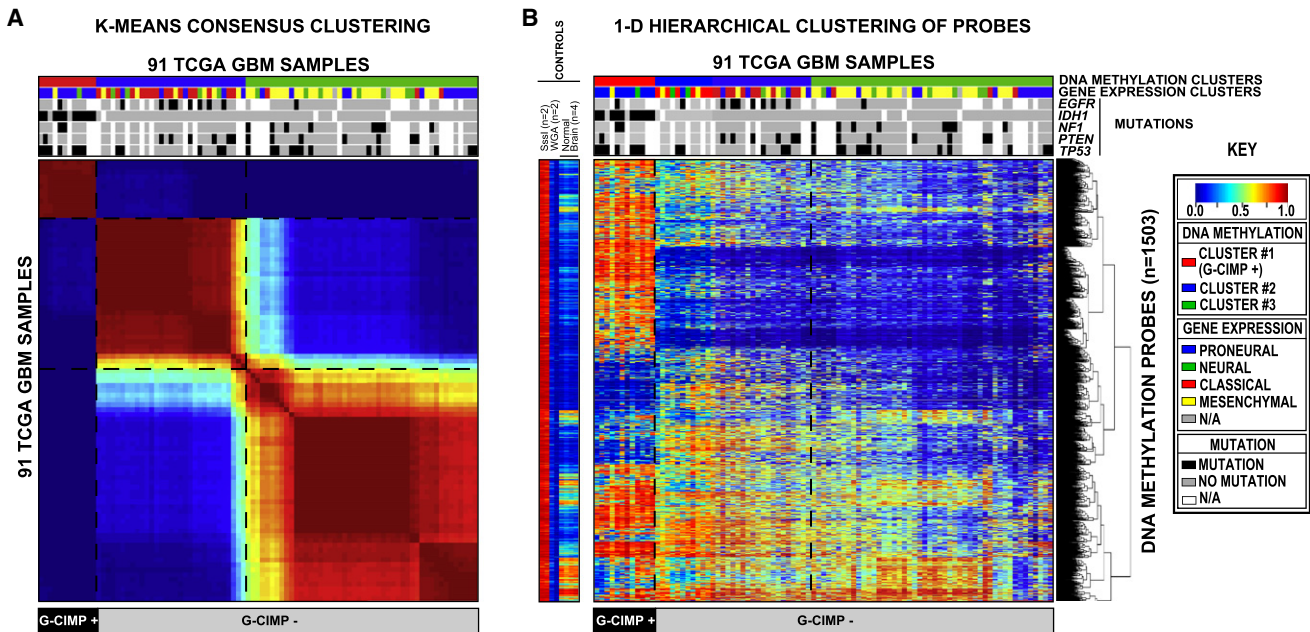


Figure 1. Clustering of TCGA GBM Tumors and Control Samples Identifies a CpG Island Methylator Phenotype

Unsupervised consensus clustering was performed with the 1503 Infinium DNA methylation probes whose DNA methylation beta values varied the most across the 91 TCGA GBM samples. DNA methylation clusters are distinguished with a color code at the top of the panel: red, consensus cluster 1 ($n = 12$ tumors); blue, consensus cluster 2 ($n = 31$ tumors); and green, consensus cluster 3 ($n = 48$ samples). Each sample within each DNA Methylation cluster are color labeled as described in the key for its gene expression cluster membership (proneural, neural, classical, and mesenchymal). The somatic mutation status of five genes (*EGFR*, *IDH1*, *NF1*, *PTEN*, and *TP53*) are indicated by the black squares, the gray squares indicate the absence of mutations in the sample, and the white squares indicate that the gene was not screened in the specific sample. G-CIMP-positive samples are labeled at the bottom of the matrix.

(A) Consensus matrix produced by k-means clustering ($K = 3$). The samples are listed in the same order on the x and y axes. Consensus index values range from 0 to 1, with 0 being highly dissimilar and 1 being highly similar.

(B) One-dimensional hierarchical clustering of the same 1503 most variant probes, with retention of the same sample order as in (A). Each row represents a probe; each column represents a sample. The level of DNA methylation (beta value) for each probe, in each sample, is represented with a color scale as shown in the legend; white indicates missing data. M.Sssl-treated DNA ($n = 2$), WGA-DNA ($n = 2$), and normal brain ($n = 4$) samples are included in the heatmap but did not contribute to the unsupervised clustering. The probes in the eight control samples are listed in the same order as the y axis of the GBM sample heatmap. See also Figure S1 and Table S1.

(Monti et al., 2003). We identified three DNA methylation clusters using either the GoldenGate or Infinium data, with 97% concordance (61/63) in cluster membership calls for samples run on both platforms (Table S1). Cluster 1 formed a particularly tight cluster on both platforms with a highly characteristic DNA methylation profile (Figure 1 and Figure S1), reminiscent of the CpG island methylator phenotype described in colorectal cancer (Toyota et al., 1999; Weisenberger et al., 2006). CIMP in colorectal cancer is characterized by correlated cancer-specific CpG island hypermethylation of a subset of genes in a subset of tumors and not just a stochastic increase in the frequency of generic CpG island methylation across the genome (Toyota et al., 1999; Weisenberger et al., 2006). Cluster 1 GBM samples show similar concerted methylation changes at a subset of loci. We therefore designated cluster 1 tumors as having a glioma CpG island methylator phenotype (G-CIMP). Combining Infinium and GoldenGate data, we identified 24 of 272 TCGA GBM samples (8.8%) as the G-CIMP subtype (Table S1).

Characterization of G-CIMP Tumors within Gene Expression Clusters

Four gene expression subtypes (proneural, neural, classical, and mesenchymal) have been previously identified and character-

ized with TCGA GBM samples (Verhaak et al., 2010). We compared the DNA methylation consensus cluster assignments for each sample to their gene expression cluster assignments (Figure 1, Figure 2A, Figures S1A and S1B, and Table S1). The G-CIMP sample cluster is highly enriched for proneural GBM tumors, whereas the DNA methylation clusters 2 and 3 are moderately enriched for classical and mesenchymal expression groups, respectively. Of the 24 G-CIMP tumors, 21 (87.5%) were classified within the proneural expression group. These G-CIMP tumors represent 30% (21/71) of all proneural GBM tumors, suggesting that G-CIMP tumors represent a distinct subset of proneural GBM tumors (Figure 2A, Figure S2A, and Table S1). The few nonproneural G-CIMP tumors belong to neural (2/24 tumors, 8.3%), and mesenchymal (1/24 tumors, 4.2%) gene expression groups.

In order to obtain an integrated view of the relationships of G-CIMP status and gene expression differences, we performed pairwise comparisons between members of different molecular subgroups (Figure 2B). We calculated the mean Euclidean distance in both DNA methylation and expression for each possible pairwise combination of the five different subtypes: G-CIMP-positive proneural, G-CIMP-negative proneural, classical, mesenchymal, and neural tumors. We observed the high

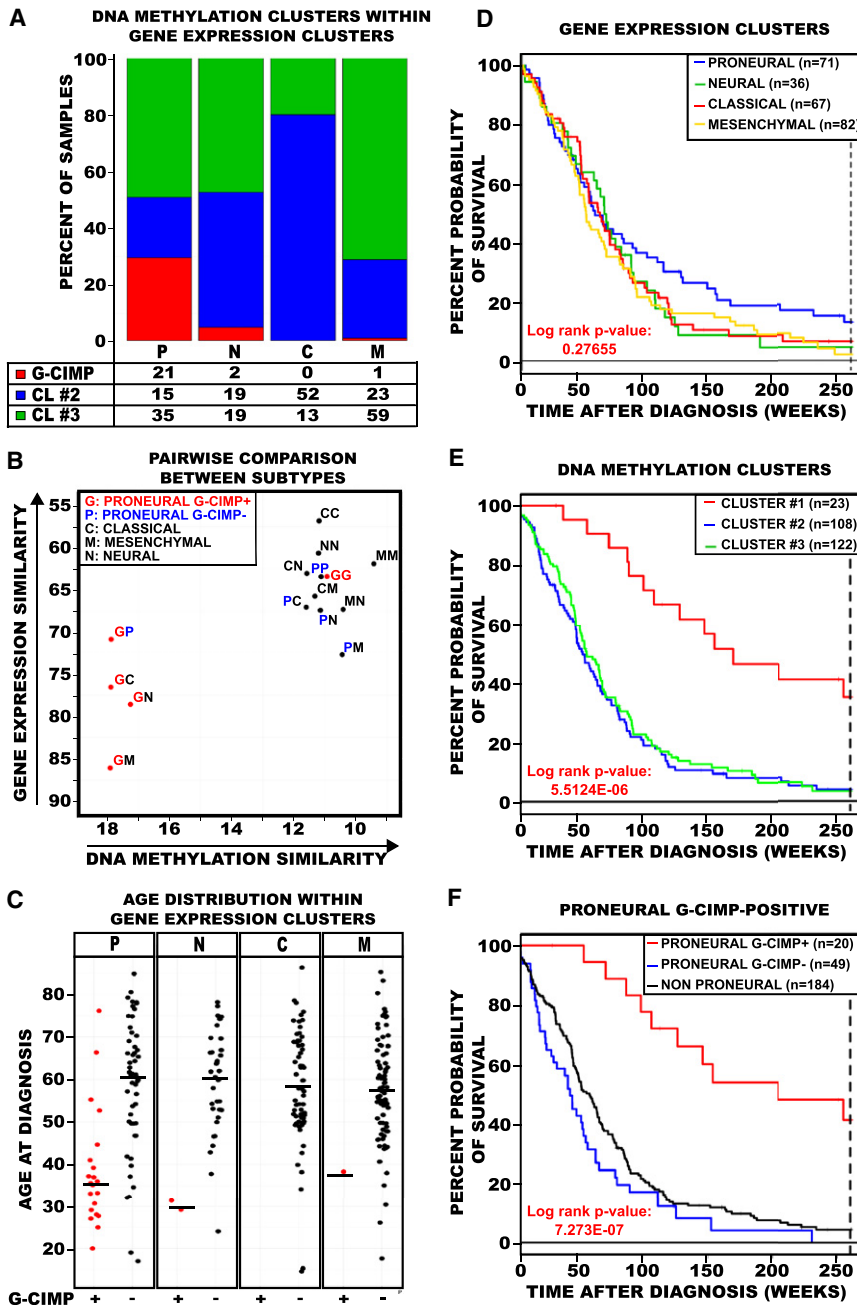


Figure 2. Characterization of G-CIMP Tumors as a Unique Subtype of GBMs within the Proneural Gene Expression Subgroup

(A) Integration of the samples within each DNA methylation and gene expression cluster. Samples are primarily categorized by their gene expression subtype: *P*, proneural; *N*, neural; *C*, classical; and *M*, mesenchymal. The number and percent of tumors within each DNA methylation cluster (red, cluster 1 [G-CIMP]; blue, cluster 2; green, cluster 3) are indicated for each gene expression subtype. (B) Scatter plot of pairwise comparison of the gene expression and DNA methylation clusters as identified in Figure 1 and Figure S1. Same two-letter represents self-comparison, whereas mixed two-letter represents the pairwise correlation between gene expression and DNA methylation. Axes are reversed to illustrate increasing similarity.

(C) GBM patient age distribution at time of diagnosis within each gene expression cluster. Samples are divided by gene expression clusters as identified along the top of each jitter plot and further subdivided by G-CIMP status within each expression subgroup. G-CIMP-positive samples are indicated as red data points and G-CIMP-negative samples are indicated as black data points. Median age at diagnosis is indicated for each subgroup by a horizontal solid black line.

(D–F) Kaplan-Meier survival curves for GBM methylation and gene expression subtypes. In each plot, the percent probability of survival is plotted versus time since diagnosis in weeks. All samples with survival data greater than 5 years were censored.

(D) Kaplan-Meier survival curves among the four GBM expression subtypes. Proneural tumors are represented in blue, neural tumors are represented in green, classical tumors are represented in red, and mesenchymal tumors are represented in gold. (E) Kaplan-Meier survival curves between the three DNA methylation clusters. Cluster 1 tumors are represented in red, cluster 2 tumors are represented in blue, and cluster 3 tumors are represented in green.

(F) Kaplan-Meier survival curves among proneural G-CIMP-positive, proneural G-CIMP-negative, and all nonproneural GBM tumors. Proneural G-CIMP-positive tumors are represented in red, proneural G-CIMP-negative tumors are represented in blue, and all nonproneural GBM tumors are represented in black. See also Figure S2.

dissimilarity of the *GP*, *GN*, *GC*, and *GM* pairs (Figure 2B), supporting the hypothesis that G-CIMP-positive tumors are a unique molecular subgroup of GBM tumors and more specifically that G-CIMP status provides further refinement of the proneural subset. Indeed, among the proneural tumors, the G-CIMP-positive tumors are distinctly dissimilar to the mesenchymal tumors (*GM* pair), whereas the G-CIMP-negative proneural tumors are relatively similar to mesenchymal tumors (*PM* pair). We focused downstream analyses on comparisons between G-CIMP-positive versus G-CIMP-negative tumors within the proneural subset, to avoid misidentifying proneural features as G-CIMP-associated features.

Clinical Characterization of G-CIMP Tumors

We further characterized G-CIMP tumors by reviewing the available clinical covariates for each patient. Although patients with proneural GBM tumors are slightly younger (median age, 56 years) than all other nonproneural GBM patients (median age, 57.5 years), this was not statistically significant ($p = 0.07$). However, patients with G-CIMP tumors were significantly younger at the time of diagnosis compared with patients diagnosed with non-G-CIMP proneural tumors (median ages of 36 and 59 years, respectively; $p < 0.0001$; Figure 2C).

The overall survival for patients of the proneural subtype was not significantly improved compared to other gene expression

Table 1. G-CIMP and *IDH1* Mutation Status in Primary, Secondary, and Recurrent GBMs

GBMs	G-CIMP		Total
	–	+	
All Tumors			
<i>IDH1</i>			
Wild-type	184	5	189
Mutant	0	18	18
Total	184	23	207
Primary Tumors			
<i>IDH1</i>			
Wild-type	171	4	175
Mutant	0	12	12
Total	171	16	187
Recurrent Tumors			
<i>IDH1</i>			
Wild-type	12	0	12
Mutant	0	4	4
Total	12	4	16
Secondary Tumors			
<i>IDH1</i>			
Wild-type	1	1	2
Mutant	0	2	2
Total	1	3	4

G-CIMP and *IDH1* mutation status are compared for All analyzed GBM tumors ($p < 2.2 \times 10^{-16}$), Primary tumors, Recurrent tumors, and Secondary tumors. P value is calculated from Fisher's exact test. See also Figure S3 and Table S2.

subtypes (Figure 2D), but significant survival differences were seen for groups defined by DNA methylation status (Figures 2E and 2F and Figure S2B). We observed significantly better survival for proneural G-CIMP-positive patients (median survival of 150 weeks) than proneural G-CIMP-negative patients (median survival of 42 weeks) or all other nonproneural GBM patients (median survivals of 54 weeks). G-CIMP status remained a significant predictor of improved patient survival ($p = 0.0165$) in Cox multivariate analysis after adjusting for patient age, recurrent versus non-recurrent tumor status and secondary GBM versus primary GBM status.

***IDH1* Sequence Alterations in G-CIMP Tumors**

Nine genes were found to have somatic mutations that were significantly associated with proneural G-CIMP-positive tumors (Figure S3A and Table S2). *IDH1* somatic mutations, recently identified primarily in secondary GBM tumors (Balss et al., 2008; Parsons et al., 2008; Yan et al., 2009), were found to be very tightly associated with G-CIMP in our data set (Table 1), with 18 *IDH1* mutations primarily observed in 23 (78%) G-CIMP-positive tumors, and 184 G-CIMP-negative tumors were *IDH1*-wild-type ($p < 2.2 \times 10^{-16}$). The five discordant cases of G-CIMP-positive, *IDH1*-wild-type tumors are not significantly different in age compared to G-CIMP-positive, *IDH1* mutant tumors (median ages of 34 and 37 years respectively; $p = 0.873$). However, the five discordant cases of G-CIMP-positive, *IDH1*-wild-type tumors are significantly younger at the time of

diagnosis compared to patients with G-CIMP-negative, *IDH1*-wild-type tumors (median ages of 37 and 59 years respectively; $p < 0.008$). Interestingly, two of the five patients each survived more than 5 years after diagnosis. We did not observe any *IDH2* mutations in the TCGA data set. Tumors displaying both G-CIMP-positive and *IDH1* mutation occurred at low frequency in primary GBM, but were enriched in the set of 16 recurrent (treated) tumors and to an even greater degree in the set of four secondary GBM (Table 1). We also identified examples of germline mutations (nine genes) and loss of heterozygosity (six genes) that were significantly associated with proneural G-CIMP-positive tumors (Figures S3B and S3C and Table S2).

DNA Copy-Number Variation in Proneural G-CIMP Tumors

In order to elucidate critical alterations within proneural G-CIMP-positive tumors, we analyzed gene-centric copy-number variation data (see Supplemental Information). We identified significant copy-number differences in 2875 genes between proneural G-CIMP-positive and G-CIMP-negative tumors (Figure 3A and Table S3). Although chromosome 7 amplifications are a hallmark of aggressive GBM tumors (The Cancer Genome Atlas Research Network, 2008), copy-number variation along chromosome 7 was reduced in proneural G-CIMP-positive tumors. Gains in chromosomes 8q23.1-q24.3 and 10p15.3-p11.21 were identified (Figures 3B and 3C). The 8q24 region contains the *MYC* oncogene, is rich in sequence variants, and was previously shown as a risk factor for several human cancers (Amundadottir et al., 2006; Freedman et al., 2006; Haiman et al., 2007a; Haiman et al., 2007b; Schumacher et al., 2007; Shete et al., 2009; Visakorpi et al., 1995; Yeager et al., 2007). Accompanying the gains at chromosome 10p in proneural G-CIMP-positive tumors, we also detected deletions of the same chromosome arm in G-CIMP-negative tumors (Figure 3C). Similar copy-number variation results were obtained when comparing all G-CIMP-positive to G-CIMP-negative samples (Figure S4). These findings point to G-CIMP-positive tumors as having a distinct profile of copy-number variation when compared to G-CIMP-negative tumors.

Identification of DNA Methylation and Transcriptome Expression Changes in Proneural G-CIMP Tumors

To better understand CpG island hypermethylation in glioblastoma, we investigated the differentially methylated CpG sites of these samples (Figure 1B). Among 3153 CpG sites that were differentially methylated between proneural G-CIMP positive and proneural G-CIMP-negative tumors, 3098 (98%) were hypermethylated (Figure 4A). In total, there were 1550 unique genes, of which 1520 were hypermethylated and 30 were hypomethylated within their promoter regions. We ranked our probe list by decreasing adjusted p values and increasing beta-value difference in order to identify the top most differentially hypermethylated CpG probes within proneural G-CIMP-positive tumors (Table S3).

The Agilent transcriptome data were used to detect genes showing both differential expression and G-CIMP DNA methylation, in G-CIMP-positive and negative proneural samples. Gene expression values were adjusted for regional copy number changes, as described in Supplemental Information. A total of

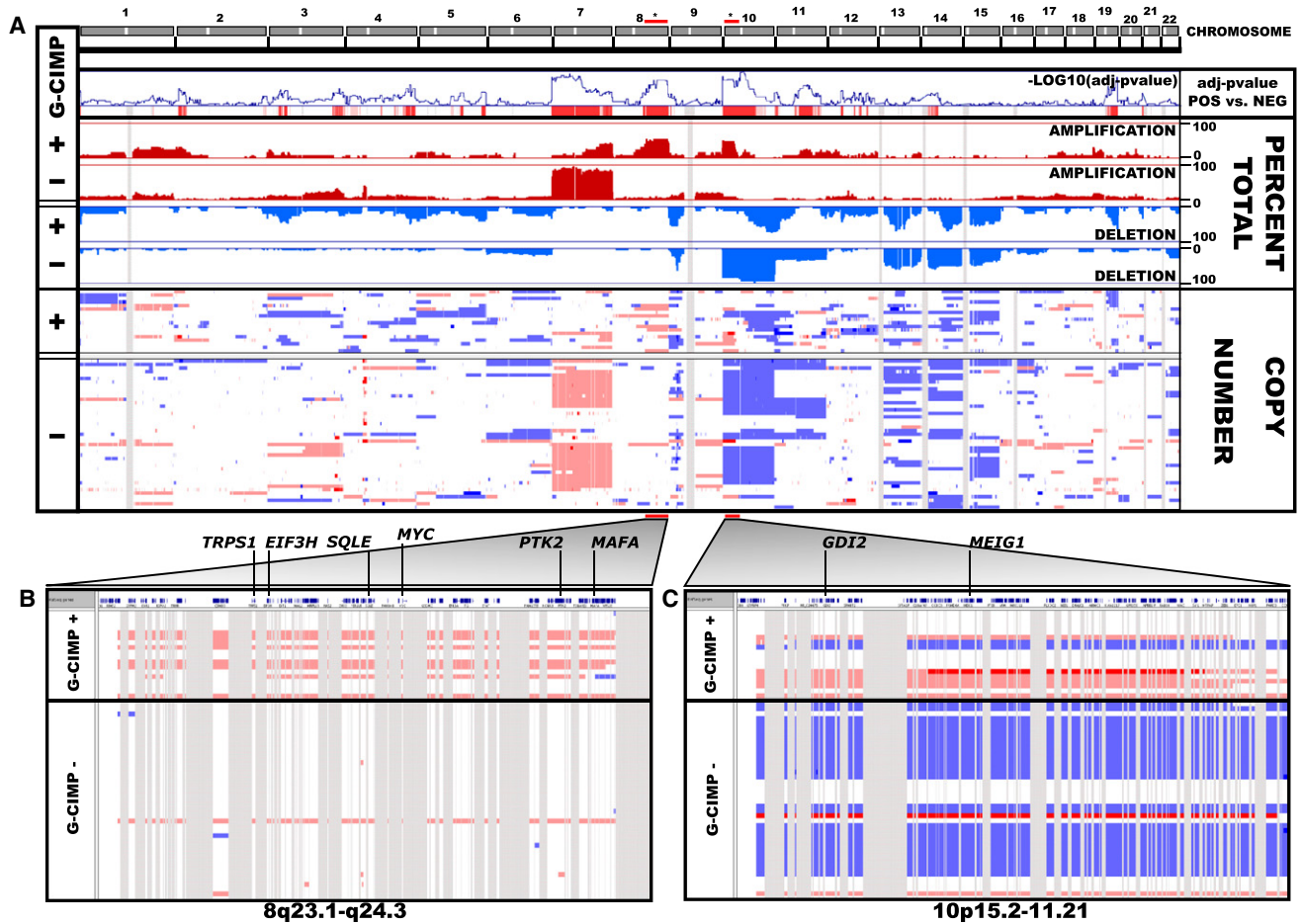


Figure 3. Significant Regions of Copy-Number Variation in the G-CIMP Genome

Copy-number variation for 23,748 loci (across 22 autosomes and plotted in genomic coordinates along the x axis) was analyzed with 61 proneural TCGA GBM tumors. Homozygous deletion is indicated in dark blue, hemizygous deletion is indicated in light blue, neutral/no change is indicated in white, gain is indicated in light red, and high-level amplification is indicated in dark red.

(A) Copy-number variation between proneural G-CIMP positive and G-CIMP negative tumors. The Cochran Armitage test for trend, percent total amplification/deletion, and raw copy-number values are listed. The $-\log_{10}(\text{FDR-adjusted } p \text{ value})$ between G-CIMP-positive and G-CIMP negative proneurals is plotted along the y axis in the “adjusted p value pos vs. neg” panel. In this panel, red vertical lines indicate significance. Gene regions in 8q23.1-q24.3 and 10p15.2-11.21 are identified by asterisks and are highlighted in (B) and (C), respectively. See also Figure S4 and Table S3.

1,030 genes were significantly downregulated and 654 genes were significantly upregulated among proneural G-CIMP-positive tumors (Figure 4B and Table S3). The differentially downregulated gene set was highly enriched for polysaccharide, heparin and glycosaminoglycan binding, collagen, thrombospondin, and cell morphogenesis ($p < 2.2\text{E-}04$, Table S3). In addition, the significantly upregulated gene set was highly enriched among functional categories involved in regulation of transcription, nucleic acid synthesis, metabolic processes, and cadherin-based cell adhesion ($p < 6.2\text{E-}04$). Zinc finger transcription factors were also found to be highly enriched in genes significantly upregulated in expression ($p = 3.1\text{E-}08$). Similar findings were obtained when a permutation analysis was performed and when Affymetrix gene expression data were used (data not shown). We also identified 20 miRNAs that showed significant differences in their gene expression between proneural G-CIMP-positive and proneural G-CIMP-negative tumors (Figure S5 and Table S3).

Integration of the normalized gene expression and DNA methylation gene lists identified a total of 300 genes with both significant DNA hypermethylation and gene expression changes in G-CIMP-positive tumors compared to G-CIMP-negative tumors within the proneural subset. Of these, 263 were significantly downregulated and hypermethylated within proneural G-CIMP-positive tumors (Figure 4C, lower-right quadrant). To validate these differentially expressed and methylated genes, we replicated the analysis using an alternate expression platform (Affymetrix) and derived consistent results (Figure S5). Among the top ranked genes were *FABP5*, *PDPN*, *CHI3L1*, and *LGALS3* (Table 2), which were identified in an independent analysis to be highly prognostic in GBM with higher expression associated with worse outcome (Colman et al., 2010). Gene ontology analyses showed G-CIMP-specific downregulation of genes associated with the mesenchyme subtype, tumor invasion, and the extracellular matrix as the most significant terms (Table S3). Genes with roles in transcriptional silencing, chromatin structure

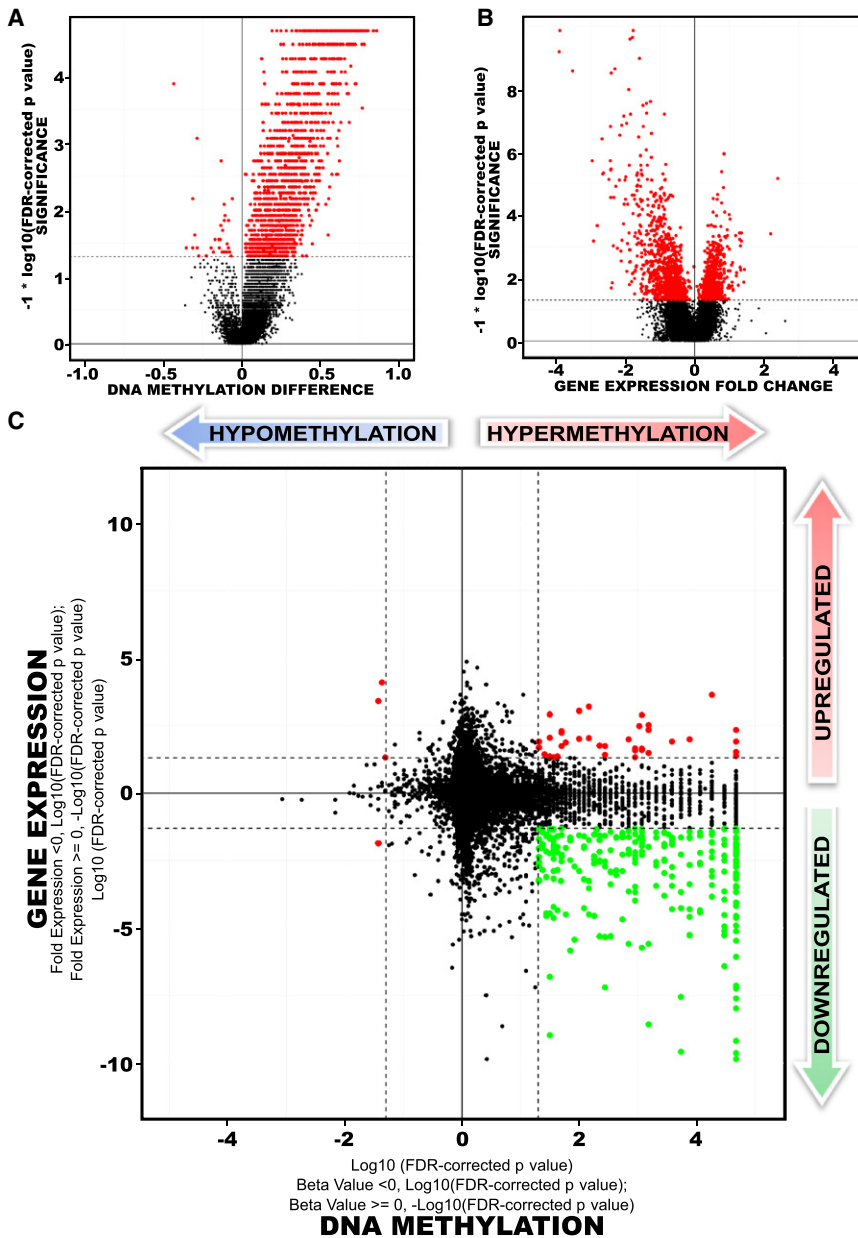


Figure 4. Comparison of Transcriptome versus Epigenetic Differences between Proneural G-CIMP-Positive and G-CIMP-Negative Tumors

(A) Volcano plots of all CpG loci analyzed for G-CIMP association. The beta value difference in DNA methylation between the proneural G-CIMP-positive and proneural G-CIMP-negative tumors is plotted on the x axis, and the p value for a FDR-corrected Wilcoxon signed-rank test of differences between the proneural G-CIMP-positive and proneural G-CIMP-negative tumors ($-1 * \log_{10}$ scale) is plotted on the y axis. Probes that are significantly different between the two subtypes are shown in red.

(B) Volcano plot for all genes analyzed on the Agilent gene expression platform.

(C) Starburst plot for comparison of TCGA Infinium DNA methylation and Agilent gene expression data normalized by copy-number information for 11,984 unique genes. \log_{10} (FDR-adjusted p value) is plotted for DNA methylation (x axis) and gene expression (y axis) for each gene. If a mean DNA methylation β -value or mean gene expression value is higher (greater than zero) in G-CIMP-positive tumors, -1 is multiplied to \log_{10} (FDR-adjusted p value), providing positive values. The dashed black lines indicate the FDR-adjusted p value at 0.05. Data points in red indicate those that are significantly up- and downregulated in their gene expression levels and significantly hypo- or hypermethylated in proneural G-CIMP-positive tumors. Data points in green indicate genes that are significantly downregulated in their gene expression levels and hypermethylated in proneural G-CIMP-positive tumors compared to proneural G-CIMP-negative tumors. See also Figure S5 and Table S3.

modifications, and activation of cellular metabolic processes showed increased gene expression in proneural G-CIMP-positive tumors. Additional genes differentially expressed in proneural G-CIMP-positive samples are provided in Table S3.

To extend these findings, we subjected the differentially silenced genes to a NextBio (www.nextbio.com) meta-analysis to identify data sets that were significantly associated with our list of 263 hypermethylated and downregulated genes. There was an overlap with downregulated genes in low- and intermediate-grade glioma compared to GBM in a variety of previously published data sets (Ducray et al., 2008; Liang et al., 2005; Sun et al., 2006) (Figure S5 and Table S3). The overlap of the 263-gene set with each of these additional datasets was unlikely to be due to chance (all analyses $p < 0.00001$). To further characterize this gene set, we tested the survival association of these

gene expression values in a collection of Affymetrix profiling data from published and publicly available sources on which clinical annotation was available. This data set included cohorts from the Rembrandt set (Madhavan et al., 2009) as well as other sources and did not include TCGA data (given that TCGA data were used to derive the gene list). In this combined data set, the expression of the 263 gene set was significantly associated with patient outcome (Figure S5G). Together, these findings suggest that G-CIMP-positive GBMs tumors have epigenetically related gene expression differences, which are more consistent with low-grade gliomas as well as high-grade tumors with favorable prognosis.

Validation of G-CIMP in GBM and Incidence in Lower-Grade Gliomas

To validate the existence of G-CIMP loci and better characterize the frequency of G-CIMP in gliomas, we used MethyLight to assay the DNA methylation levels in eight G-CIMP gene regions in seven hypermethylated loci (*ANKRD43*, *HFE*, *MAL*, *LGALS3*, *FAS-1*, *FAS-2*, and *RHO-F*) and one hypomethylated locus,

Table 2. The Top-50 Most Differentially Hypermethylated and Downregulated Genes in Proneural G-CIMP-Positive Tumors

Gene Name	DNA Methylation		Gene Expression	
	Wilcoxon Rank p Value	Beta Value Difference	Wilcoxon Rank p Value	Fold Change
<i>G0S2</i>	2.37E-07	0.76	2.12E-13	-3.92
<i>RBP1</i>	2.37E-07	0.84	1.07E-14	-3.9
<i>FABP5</i>	2.30E-05	0.3	1.39E-12	-3.53
<i>CA3</i>	4.50E-06	0.43	2.06E-06	-2.82
<i>RARRS2</i>	4.74E-07	0.63	6.25E-10	-2.69
<i>OCIAD2</i>	2.06E-04	0.32	1.23E-08	-2.64
<i>CBR1</i>	3.30E-05	0.37	3.77E-09	-2.45
<i>PDPN</i>	3.87E-03	0.23	1.47E-07	-2.43
<i>LGALS3</i>	2.37E-07	0.72	7.97E-09	-2.42
<i>CTHRC1</i>	3.50E-04	0.45	1.44E-07	-2.34
<i>CCNA1</i>	4.66E-03	0.29	2.95E-05	-2.14
<i>ARMC3</i>	1.76E-03	0.31	7.76E-05	-2.13
<i>CHST6</i>	5.74E-04	0.22	8.70E-06	-2.11
<i>C11orf63</i>	2.37E-07	0.64	7.95E-11	-2.05
<i>GJB2</i>	2.16E-03	0.24	2.94E-07	-2.04
<i>KIAA0746</i>	1.66E-06	0.58	2.97E-07	-1.94
<i>MOSC2</i>	2.37E-07	0.66	6.85E-12	-1.91
<i>CHI3L1</i>	7.11E-06	0.13	4.11E-06	-1.9
<i>RARRS1</i>	6.38E-05	0.41	5.93E-09	-1.89
<i>AQP5</i>	4.50E-06	0.43	6.86E-14	-1.87
<i>SPON2</i>	8.68E-05	0.3	2.50E-05	-1.87
<i>RAB36</i>	2.06E-04	0.26	6.49E-11	-1.86
<i>CHRD12</i>	2.64E-03	0.07	1.15E-07	-1.81
<i>TOM1L1</i>	2.37E-07	0.66	4.57E-14	-1.8
<i>BIRC3</i>	2.37E-07	0.66	6.50E-07	-1.78
<i>LDHA</i>	4.50E-04	0.55	1.83E-07	-1.74
<i>SEMA3E</i>	2.37E-07	0.52	2.36E-04	-1.72
<i>FMOD</i>	6.38E-05	0.42	2.05E-04	-1.72
<i>C10orf107</i>	1.59E-05	0.63	4.11E-06	-1.71
<i>FLNC</i>	2.37E-07	0.74	1.36E-05	-1.67
<i>TMEM22</i>	4.74E-07	0.59	1.63E-08	-1.67
<i>TCTEX1D1</i>	1.66E-06	0.37	2.97E-07	-1.67
<i>DKFZP586H2123</i>	1.59E-05	0.53	4.83E-05	-1.66
<i>TRIP4</i>	4.74E-07	0.49	4.18E-08	-1.65
<i>SLC39A12</i>	1.81E-03	0.2	7.24E-06	-1.65
<i>FLJ21963</i>	4.60E-05	0.26	8.07E-07	-1.63
<i>CRYGD</i>	4.74E-07	0.54	2.81E-08	-1.62
<i>LECT1</i>	5.74E-04	0.32	3.73E-07	-1.61
<i>EPHX2</i>	2.37E-07	0.53	3.73E-06	-1.6
<i>LGALS8</i>	3.20E-03	0.19	4.15E-13	-1.6
<i>C7orf46</i>	2.37E-07	0.35	4.11E-06	-1.58
<i>F3</i>	2.37E-07	0.62	4.76E-08	-1.57
<i>TTC12</i>	9.48E-07	0.53	4.52E-06	-1.57
<i>ITGBL1</i>	1.42E-03	0.2	1.86E-07	-1.57
<i>B3GNT5</i>	1.66E-06	0.66	2.36E-07	-1.55
<i>NMNAT3</i>	2.30E-05	0.62	5.93E-09	-1.55

Table 2. Continued

Gene Name	DNA Methylation		Gene Expression	
	Wilcoxon Rank p Value	Beta Value Difference	Wilcoxon Rank p Value	Fold Change
<i>FZD6</i>	6.38E-05	0.34	2.28E-06	-1.55
<i>FKBP5</i>	9.16E-04	0.23	9.22E-09	-1.54
<i>SLC25A20</i>	1.56E-04	0.6	1.41E-08	-1.53
<i>MMP9</i>	2.06E-04	0.37	2.09E-03	-1.53

Genes are sorted by decreasing Gene Expression \log_2 ratios. Beta value difference indicates differences in mean of beta values (DNA methylation values) between proneural G-CIMP-positive and proneural G-CIMP-negative tumors. Fold change is the \log_2 ratio of the means of proneural G-CIMP-positive and proneural G-CIMP-negative normalized expression intensities. See also Table S3.

DOCK5, in the tumor samples. These eight markers were evaluated in paraffin-embedded tissues from 20 TCGA samples of known G-CIMP status (ten G-CIMP-positive and ten G-CIMP-negative). We observed perfect concordance between G-CIMP calls on the array platforms and those with the MethyLight markers, providing validation of the technical performance of the platforms and of the diagnostic marker panel. These 20 samples were excluded from the validation set described below. A sample was considered G-CIMP positive if at least six genes displayed a combination of *DOCK5* DNA hypomethylation and/or hypermethylation of the remaining genes in the panel. Using these criteria, we tested an independent set of non-TCGA GBM samples for G-CIMP status. Sixteen of 208 tumors (7.6%) were found to be G-CIMP positive (Figure 5A), very similar to the findings in TCGA data.

To further expand these observations, we determined the *IDH1* mutation status for an independent set 100 gliomas (WHO grades II, III, and IV). Among 48 *IDH1* mutant tumors, 35 (72.9%) were positive for G-CIMP. However, only 3/52 cases (5.8%) without an *IDH1* mutation were G-CIMP positive (odds ratio = 42; 95% confidence interval (CI), 11-244; Figure S3D), validating the tight association of G-CIMP and *IDH1* mutation.

On the basis of the association of G-CIMP status with features of the progressive, rather than the de novo GBM pathway, we hypothesized that G-CIMP status was more common in the low- and intermediate-grade gliomas. We extended this analysis by evaluating 60 grade II and 92 grade III gliomas for G-CIMP DNA methylation using the eight gene MethyLight panel. Compared to GBM, grade II tumors showed a ~10-fold increase in G-CIMP-positive tumors, whereas grade III tumors had an intermediate proportion of tumors that were G-CIMP positive (Figure 5A and Figure S3E). When low- and intermediate-grade gliomas were separated by histologic type, G-CIMP positivity appeared to be approximately twice as common in oligodendrogliomas (52/56, 93%) as compared to astrocytomas (43/95, 45%). G-CIMP positive status correlated with improved patient survival within each WHO-recognized grade of diffuse glioma, indicating that the G-CIMP status was prognostic for glioma patient survival ($p < 0.032$, Figure 5B). G-CIMP status was an independent predictor ($p < 0.01$) of survival after adjustment for patient age and tumor grade (Figure S3F). Together, these

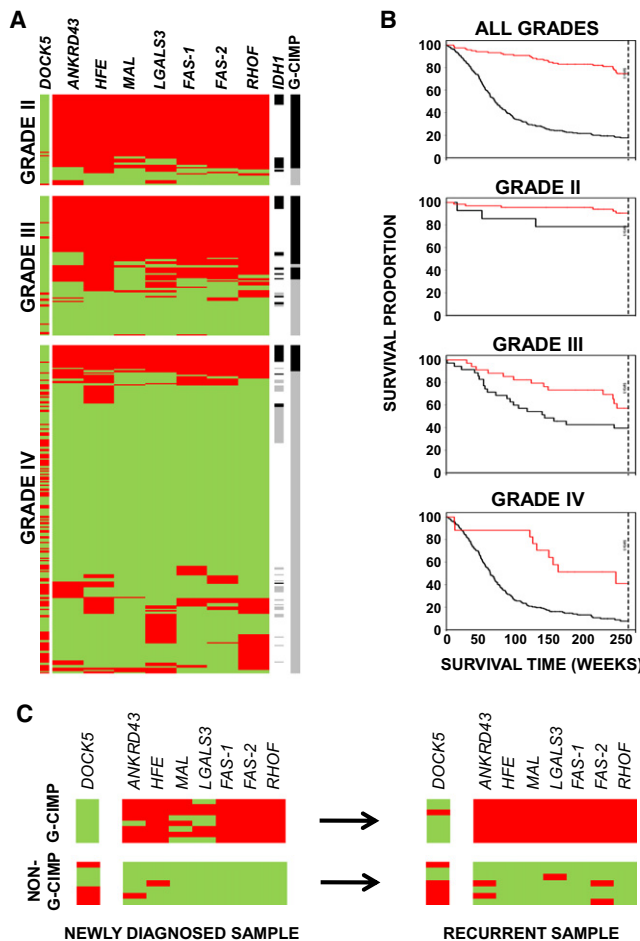


Figure 5. G-CIMP Prevalence in Grade II, III, and IV Gliomas with MethyLight

(A) Methylation profiling of gliomas shows an association of CIMP status with tumor grade. Eight markers were tested for G-CIMP DNA methylation in 360 tumor samples. Each marker was coded as red if methylated and green if unmethylated. One of these markers (*DOCK5*) is unmethylated in CIMP, whereas the remaining seven markers show G-CIMP-specific hypermethylation. G-CIMP-positive status was determined if ≥ 6 of the 8 genes had G-CIMP-defining hyper- or hypomethylation. G-CIMP-positive status is indicated with a black line (right side of panel), and a gray line indicates non-G-CIMP. Samples with an identified *IDH1* mutation are indicated by black lines and samples with no known *IDH1* mutation are indicated by gray lines. White lines indicate samples with unknown *IDH1* status.

(B) Association of G-CIMP status with patient outcome stratified by tumor grade. G-CIMP-positive cases are indicated by red lines and the G-CIMP-negative cases are indicated by black lines in each Kaplan-Meier survival curve.

(C) Stability of G-CIMP over time in glioma patients. Fifteen samples from newly diagnosed tumors were tested for G-CIMP positivity with the eight-marker MethyLight panel. Eight tumors were classified as G-CIMP-positive (upper left), and seven tumors were classified as G-CIMP-negative (non-G-CIMP, lower left). Samples from a second procedure, ranging from 2–9 years after the initial resection, were also evaluated for the G-CIMP-positive cases (upper right), as well as for the non-G-CIMP cases (lower right). Each marker was coded as red if methylated and green if unmethylated.

findings show that G-CIMP is a prevalent molecular signature in low-grade gliomas and confers improved survival in these tumors.

Stability of G-CIMP at Recurrence

Because epigenetic events can be dynamic processes, we examined whether G-CIMP status was a stable event in glioma or whether it was subject to change over the course of the disease. To test this, we obtained a set of samples from 15 patients who received a second surgical procedure after tumor recurrence, with time intervals of up to 8 years between initial and second surgical procedures. We used the eight-gene MethyLight panel to determine their G-CIMP status and found that eight samples were G-CIMP positive, whereas seven were G-CIMP negative. Interestingly, among the G-CIMP-positive cases, 8/8 (100%) recurrent samples retained their G-CIMP-positive status. Similarly, among seven G-CIMP-negative cases, all seven remained G-CIMP negative at recurrence, indicating stability of the G-CIMP phenotype over time (Figure 5C).

DISCUSSION

In this report, we have identified and characterized a distinct molecular subgroup in human gliomas. Analysis of epigenetic changes from TCGA samples identified the existence of a proportion of GBM tumors with highly concordant DNA methylation of a subset of loci, indicative of a CpG island methylator phenotype (G-CIMP). G-CIMP-positive samples were associated with secondary or recurrent (treated) tumors and tightly associated with *IDH1* mutation. G-CIMP tumors also showed a relative lack of copy-number variation commonly observed in GBM, including *EGFR* amplification, chromosome 7 gain, and chromosome 10 loss. Interestingly, G-CIMP tumors displayed copy-number alterations that were also shown in gliomas with *IDH1* mutations in a recent report (Sanson et al., 2009). Integration of the DNA methylation data with gene expression data showed that G-CIMP-positive tumors represent a subset of proneural tumors. G-CIMP-positive tumors showed a favorable prognosis within GBMs as a whole and also within the proneural subset, consistent with prior reports for *IDH1* mutant tumors (Parsons et al., 2008; Yan et al., 2009). Interestingly, of the five discordant cases of G-CIMP-positive, *IDH1*-wild-type tumors, two patients survived more than 5 years after diagnosis, suggesting that G-CIMP-positive status may confer favorable outcome independent of *IDH1* mutation status. However, studies with many more discordant cases will be needed to carefully dissect the effects of G-CIMP status versus *IDH1* mutation on survival. To a large extent, the improved prognosis conferred by proneural tumors (Phillips et al., 2006) can be accounted for by the G-CIMP-positive subset. These findings indicate that G-CIMP could be used to further refine the expression-defined groups into an additional subtype with clinical implications.

G-CIMP is highly associated with *IDH1* mutation across all glioma tumor grades, and the prevalence of both decreases with increasing tumor grade. Tumor grade is defined by morphology only and therefore can be heterogeneous with respect to molecular subtypes. Within grade IV/glioblastoma tumors are a subset of patients who tend to be younger and have a relatively favorable prognosis. It is only through molecular characterization with markers such as *IDH1* and G-CIMP status that one could prospectively identify such patients. Conversely, these markers could also be used to identify patients with

low- and intermediate-grade gliomas who may exhibit unfavorable outcome relative to tumor grade.

In the non-TCGA independent validation set examined in this study, an *IDH1* mutation was detected in 40/43 (93%) low- and intermediate-grade gliomas, but only 7/57 (13%) of primary GBMs. Similarly, we detected nearly 10-fold more G-CIMP-positive gliomas in grade II tumors as compared to grade IV GBMs. The improved survival of G-CIMP gliomas at all tumor grades suggests that there are molecular features within G-CIMP gliomas that encourage a less aggressive tumor phenotype. Consistent with this, we identified G-CIMP-specific DNA methylation changes within a broad panel of genes whose expression was significantly associated with patient outcome. We observed that this large subset of differentially silenced genes was involved in specific functional categories, including markers of mesenchyme, tumor invasion, and extracellular matrix. This concept builds upon our prior finding of a mesenchymal subgroup of glioma which shows poor prognosis (Phillips et al., 2006). According to this model, a lack of methylation of these genes in G-CIMP-negative tumors would result in a relative increase in expression of these genes, which in turn would promote tumor progression and/or lack of response to currently available treatment modalities. A comparison of the G-CIMP gene list with prior gene expression analyses (meta-analyses) suggests that G-CIMP positive tumors may be less aggressive because of silencing of key mesenchymal genes.

We found that a minority of genes with significant promoter hypermethylation showed a concomitant significant decrease in associated gene expression (263/1520, 17%). This is consistent with previous reports, in which we found similarly low frequencies of inversely correlated promoter hypermethylation and gene expression (Houshdaran et al., 2010; Pike et al., 2008). The lack of an inverse relationship between promoter hypermethylation and gene expression for most genes may be attributed to several scenarios, including the lack of appropriate transcription factors for some unmethylated genes and the use of alternative promoters for some genes with methylated promoters. Epigenetics controls expression potential, rather than expression state.

RBP1 and *GOS2* are the two genes showing the strongest evidence for epigenetic silencing in G-CIMP tumors. *RBP1* has been previously reported to be epigenetically silenced in cancer cell lines and primary tumors, and the association of its encoded protein with retinoic acid receptors (RARs) has been well characterized (Esteller et al., 2002). *GOS2* gene expression is regulated by retinoic acid (RA) and encodes a protein that promotes apoptosis in primary cells, suggesting a tumor-suppressor role (Kitareewan et al., 2008; Welch et al., 2009). The vitamin A metabolite RA is important for both embryonic and adult growth. RA has diverse roles involving neuronal development and differentiation mediated by RARs (reviewed in Malik et al., 2000). Interestingly, studies in breast cancer cells have shown that silencing of *RBP1* plays an important role in RA signaling by lowering all-*trans*-retinoic acid production and loss of RAR levels and activity mediated by derepression of PI3K/Akt signaling pathway, leading to loss of cell differentiation and tumor progression (Farias et al., 2005a; Farias et al., 2005b). This mechanism may help describe the molecular features of tumorigenesis in G-CIMP tumors. Thus, dissecting the gene

expression and DNA methylation alterations of G-CIMP tumors among lower-grade gliomas will be helpful for better understanding of the roles of a mutant *IDH1* and G-CIMP DNA methylation on tumor grade and patient survival.

The highly concerted nature of G-CIMP methylation suggests that this phenomenon may be caused by a defect in a *trans*-acting factor normally involved in the protection of a defined subset of CpG island promoters from encroaching DNA methylation. Loss of function of this factor would result in widespread concerted DNA methylation changes. We propose that transcriptional silencing of some CIMP genes may provide a favorable context for the acquisition of specific genetic lesions. Indeed, we have recently found that *IGFBP7* is silenced by promoter hypermethylation in *BRAF* mutant CIMP+ colorectal tumors (Hinoue et al., 2009). Oncogene-induced senescence by mutant *BRAF* is known to be mediated by *IGFBP7* (Wajapeyee et al., 2008). Hence, CIMP-mediated inactivation of *IGFBP7* provides a suitable environment for the acquisition of *BRAF* mutation. The tight concordance of G-CIMP status with *IDH1* mutation in GBM tumors is very reminiscent of colorectal CIMP, in which DNA hypermethylation is strongly associated with *BRAF* mutation (Weisenberger et al., 2006). We hypothesize that the transcriptional silencing of as yet unknown G-CIMP targets may provide an advantageous environment for the acquisition of *IDH1* mutation.

In our integrative analysis of G-CIMP tumors, we observed upregulation of genes functionally related to cellular metabolic processes and positive regulation of macromolecules. This expression profile may reflect a metabolic adjustment to the proliferative state of the tumor, in conjunction with the gain-of-function *IDH1* mutation (Dang et al., 2009). Such a metabolic adjustment may be consistent with Warburg's observation that proliferating normal and tumor cells require both biomass and energy production and convert glucose primarily to lactate, regardless of oxygen levels, whereas nonproliferating differentiated cells emphasize efficient energy production (reviewed in Vander Heiden et al., 2009).

In summary, our data indicate that G-CIMP status stratify gliomas into two distinct subgroups with different molecular and clinical phenotypes. These molecular classifications have implications for differential therapeutic strategies for glioma patients. Further observation and characterization of molecular subsets will probably provide additional information enabling insights into the the development and progression of glioma, and may lead to targeted drug treatment for patients with these tumors.

EXPERIMENTAL PROCEDURES

Samples and DNA Methylation Assays

Genomic DNAs from TCGA GBM tumors were isolated by the TCGA Biospecimen Core Resource (BCR) and delivered to USC as previously described (The Cancer Genome Atlas Research Network, 2008). One sample (TCGA-06-0178) with a confirmed *IDH1* mutation was removed from our analyses, given that it became clear that an incorrect tissue type had been shipped for the DNA methylation analysis. Four brain genomic DNA samples from apparently healthy individuals were included as controls. All tissue samples (patients and healthy individuals) were obtained with institutional review board-approved protocols from University of Southern California (TCGA GBM samples), Johns Hopkins School of Medicine (normal brain samples), and

The University of Texas MD Anderson Cancer Center (glioma validation samples). Tissue samples were deidentified so that patient confidentiality was ensured. Genomic DNA methylated *in vitro* with M.SssI methylase or whole-genome amplified (WGA) as positive and negative controls for DNA methylation, respectively, were also included. Details are in the [Supplemental Information](#).

The GoldenGate assays were performed according to the manufacturer's instructions and as described previously (Bibikova *et al.*, 2006). The GoldenGate methylation assays survey the DNA methylation of up to 1536 CpG sites—a total of 1505 CpGs spanning 807 unique gene loci are interrogated in the OMA-002 probe set (Bibikova *et al.*, 2006), and 1498 CpGs spanning the same number of unique gene regions are investigated in the OMA-003 probe set (The Cancer Genome Atlas Research Network, 2008).

The Infinium methylation assays were performed in accordance with the manufacturer's instructions. The assay generates DNA methylation data for 27,578 CpG dinucleotides spanning 14,473 well-annotated, unique gene promoter and/or 5' gene regions (from -1,500 to +1,500 from the transcription start site). The assay information is available at www.illumina.com and the probe information is available on the TCGA Data Portal website. Data from 91 TCGA GBM samples (batches 1, 2, 3, and 10) were included in this analysis. Batches 1–3 (63 samples) were run on both Infinium and GoldenGate, whereas batches 4–8 (182 samples) were analyzed exclusively on GoldenGate, and batch 10 (28 samples) was analyzed exclusively on Infinium. All data were packaged and deposited onto the TCGA Data Portal website (<http://tcga.cancer.gov/dataportal>). [Figure S1C](#) illustrates a Venn diagram with the overlapping samples between different DNA methylation platforms. Additional details on DNA methylation detection protocols and TCGA GBM data archived versions are in the [Supplemental Information](#).

Integrative TCGA Data Platforms

Although ancillary data (expression, mutation, and copy number) were available for additional tumor samples, we only included those samples for which there were DNA methylation profiling (either GoldenGate or Infinium). Given that the Agilent gene expression platform contained a greater number of genes for which DNA methylation data were available, we limited our primary analysis to only the Agilent gene expression data set. Where appropriate, we confirmed results using the Affymetrix gene expression data. Additional details are in the [Supplemental Information](#).

Clustering Analysis and Measurement of Differential DNA Methylation and Differential Gene Expression

Probes for each platform were filtered by removal of those targeting the X and Y chromosomes, those containing a single-nucleotide polymorphism (SNP) within five base pairs of the targeted CpG site, and probes containing repeat element sequences ≥ 10 base pairs. We next retained the most variably methylated probes (standard deviation > 0.20) across the tumor set in each DNA methylation platform. These final data matrices were used for unsupervised Consensus/Hierarchical clustering analyses. A nonparametric approach (Wilcoxon rank-sum test) was used for determining probes/genes that are differentially DNA methylated or differentially expressed between the two groups of interest. Additional information is described in the [Supplemental Information](#).

G-CIMP Validation with MethyLight Technology

Tumor samples were reviewed by a neuropathologist (K.A.) to ensure accuracy of diagnosis as well as quality control to minimize normal tissue contamination. MethyLight real-time PCR strategy was performed as described previously (Eads *et al.*, 2000; Eads *et al.*, 1999). Additional details are in the [Supplemental Information](#).

Pathway and Meta-analyses and Statistical Analyses

Additional tools included the Molecular Signatures Database (MSigDB database v2.5), Database for Annotation, Visualization, and Integrated Discovery (DAVID) and NextBio. All statistical tests were done with R software (R version 2.9.2, 2009-08-24, (R Development Core Team, 2009) and packages in Bioconductor (Gentleman *et al.*, 2004), except as noted. Additional details are in the [Supplemental Information](#).

SUPPLEMENTAL INFORMATION

Supplemental Information includes five figures, three tables, Supplemental Experimental Procedures, and a list of authors and affiliations of the TCGA Research Network and can be found with this article online at [doi:10.1016/j.ccr.2010.03.017](https://doi.org/10.1016/j.ccr.2010.03.017).

ACKNOWLEDGMENTS

This work was supported by NIH/NCI grants U24 CA126561 and U24 CA143882-01 (P.W.L. and S.B.B.), grants from the M.D. Anderson Center for Cancer Epigenetics, the Brain Tumor Funders' Collaborative, the V Foundation, and the Rose Foundation, and SPORE grant P50CA127001 from NIH/NCI (K.A.). We thank Dennis Maglinte and members of the USC Epigenome Center for helpful discussions, Andreana Rivera for technical assistance, and Marisol Guerrero for editorial assistance. P.W.L. is a shareholder, consultant, and scientific advisory board member of Epigenomics, AG, which has a commercial interest in DNA methylation markers. This work was not supported by Epigenomics, AG. K.A. is a consultant and scientific advisory board member for Castle Biosciences, which has a commercial interest in molecular diagnostics. This work was not supported by Castle Biosciences.

Received: December 8, 2009

Revised: February 18, 2010

Accepted: March 30, 2010

Published online: April 15, 2010

REFERENCES

- Adamson, C., Kanu, O.O., Mehta, A.I., Di, C., Lin, N., Mattox, A.K., and Bigner, D.D. (2009). Glioblastoma multiforme: A review of where we have been and where we are going. *Expert Opin. Investig. Drugs* 18, 1061–1083.
- Amundadottir, L.T., Sulem, P., Gudmundsson, J., Helgason, A., Baker, A., Agnarsson, B.A., Sigurdsson, A., Benediktsson, K.R., Cazier, J.B., Sainz, J., *et al.* (2006). A common variant associated with prostate cancer in European and African populations. *Nat. Genet.* 38, 652–658.
- Bals, J., Meyer, J., Mueller, W., Korshunov, A., Hartmann, C., and von Deimling, A. (2008). Analysis of the IDH1 codon 132 mutation in brain tumors. *Acta Neuropathol.* 116, 597–602.
- Bibikova, M., Lin, Z., Zhou, L., Chudin, E., Garcia, E.W., Wu, B., Doucet, D., Thomas, N.J., Wang, Y., Vollmer, E., *et al.* (2006). High-throughput DNA methylation profiling using universal bead arrays. *Genome Res.* 16, 383–393.
- Bleeker, F.E., Lamba, S., Leenstra, S., Troost, D., Hulsebos, T., Vandertop, W.P., Frattini, M., Molinari, F., Knowles, M., Cerrato, A., *et al.* (2009). IDH1 mutations at residue p.R132 (IDH1(R132)) occur frequently in high-grade gliomas but not in other solid tumors. *Hum. Mutat.* 30, 7–11.
- Brandes, A.A., Ermani, M., Basso, U., Amistà, P., Berti, F., Scienza, R., Rotilio, A., Pinna, G., Gardiman, M., and Monfardini, S. (2001). Temozolomide as a second-line systemic regimen in recurrent high-grade glioma: A phase II study. *Ann. Oncol.* 12, 255–257.
- Cahill, D.P., Levine, K.K., Betensky, R.A., Codd, P.J., Romany, C.A., Reavie, L.B., Batchelor, T.T., Futreal, P.A., Stratton, M.R., Curry, W.T., *et al.* (2007). Loss of the mismatch repair protein MSH6 in human glioblastomas is associated with tumor progression during temozolomide treatment. *Clin. Cancer Res.* 13, 2038–2045.
- The Cancer Genome Atlas Research Network (2008). Comprehensive genomic characterization defines human glioblastoma genes and core pathways. *Nature* 455, 1061–1068.
- Canoll, P., and Goldman, J.E. (2008). The interface between glial progenitors and gliomas. *Acta Neuropathol.* 116, 465–477.
- Colman, H., Zhang, L., Sulman, E.P., McDonald, J.M., Shooshtari, N.L., Rivera, A., Popoff, S., Nutt, C.L., Louis, D.N., Cairncross, J.G., *et al.* (2010). A multi-gene predictor of outcome in glioblastoma. *Neuro-oncol.* 12, 49–57.
- Dang, L., White, D.W., Gross, S., Bennett, B.D., Bittinger, M.A., Driggers, E.M., Fantin, V.R., Jang, H.G., Jin, S., Keenan, M.C., *et al.* (2009). Cancer-associated IDH1 mutations produce 2-hydroxyglutarate. *Nature* 462, 739–744.

- Dirks, P.B. (2006). Cancer: Stem cells and brain tumours. *Nature* **444**, 687–688.
- Ducray, F., Idbaih, A., de Reyniès, A., Bièche, I., Thillet, J., Mokhtari, K., Lair, S., Marie, Y., Paris, S., Vidaud, M., et al. (2008). Anaplastic oligodendrogliomas with 1p19q codeletion have a proneural gene expression profile. *Mol. Cancer* **7**, 41.
- Eads, C.A., Danenberg, K.D., Kawakami, K., Saltz, L.B., Danenberg, P.V., and Laird, P.W. (1999). CpG island hypermethylation in human colorectal tumors is not associated with DNA methyltransferase overexpression. *Cancer Res.* **59**, 2302–2306.
- Eads, C.A., Danenberg, K.D., Kawakami, K., Saltz, L.B., Blake, C., Shibata, D., Danenberg, P.V., and Laird, P.W. (2000). MethyLight: A high-throughput assay to measure DNA methylation. *Nucleic Acids Res.* **28**, E32.
- Eckhardt, F., Lewin, J., Cortese, R., Rakan, V.K., Attwood, J., Burger, M., Burton, J., Cox, T.V., Davies, R., Down, T.A., et al. (2006). DNA methylation profiling of human chromosomes 6, 20 and 22. *Nat. Genet.* **38**, 1378–1385.
- Esteller, M., Hamilton, S.R., Burger, P.C., Baylin, S.B., and Herman, J.G. (1999). Inactivation of the DNA repair gene O6-methylguanine-DNA methyltransferase by promoter hypermethylation is a common event in primary human neoplasia. *Cancer Res.* **59**, 793–797.
- Esteller, M., Garcia-Foncillas, J., Andion, E., Goodman, S.N., Hidalgo, O.F., Vanaclocha, V., Baylin, S.B., and Herman, J.G. (2000). Inactivation of the DNA-repair gene MGMT and the clinical response of gliomas to alkylating agents. *N. Engl. J. Med.* **343**, 1350–1354.
- Esteller, M., Guo, M., Moreno, V., Peinado, M.A., Capella, G., Galm, O., Baylin, S.B., and Herman, J.G. (2002). Hypermethylation-associated inactivation of the cellular retinoid-binding-protein 1 gene in human cancer. *Cancer Res.* **62**, 5902–5905.
- Farias, E.F., Marzan, C., and Mira-y-Lopez, R. (2005a). Cellular retinoid-binding protein-1 inhibits PI3K/Akt signaling through a retinoic acid receptor-dependent mechanism that regulates p85-p110 heterodimerization. *Oncogene* **24**, 1598–1606.
- Farias, E.F., Ong, D.E., Ghyselinck, N.B., Nakajo, S., Kuppumbatti, Y.S., and Mira y Lopez, R. (2005b). Cellular retinoid-binding protein I, a regulator of breast epithelial retinoic acid receptor activity, cell differentiation, and tumorigenicity. *J. Natl. Cancer Inst.* **97**, 21–29.
- Freedman, M.L., Haiman, C.A., Patterson, N., McDonald, G.J., Tandon, A., Waliszewska, A., Penney, K., Steen, R.G., Ardlie, K., John, E.M., et al. (2006). Admixture mapping identifies 8q24 as a prostate cancer risk locus in African-American men. *Proc. Natl. Acad. Sci. USA* **103**, 14068–14073.
- Furnari, F.B., Fenton, T., Bachoo, R.M., Mukasa, A., Stommel, J.M., Stegh, A., Hahn, W.C., Ligon, K.L., Louis, D.N., Brennan, C., et al. (2007). Malignant astrocytic glioma: Genetics, biology, and paths to treatment. *Genes Dev.* **21**, 2683–2710.
- Galli, R., Binda, E., Orfanelli, U., Cipelletti, B., Gritti, A., De Vitis, S., Fiocco, R., Foroni, C., Dimeco, F., and Vescovi, A. (2004). Isolation and characterization of tumorigenic, stem-like neural precursors from human glioblastoma. *Cancer Res.* **64**, 7011–7021.
- Gentleman, R.C., Carey, V.J., Bates, D.M., Bolstad, B., Dettling, M., Dudoit, S., Ellis, B., Gautier, L., Ge, Y., Gentry, J., et al. (2004). Bioconductor: Open software development for computational biology and bioinformatics. *Genome Biol.* **5**, R80.
- Haiman, C.A., Le Marchand, L., Yamamoto, J., Stram, D.O., Sheng, X., Kolonel, L.N., Wu, A.H., Reich, D., and Henderson, B.E. (2007a). A common genetic risk factor for colorectal and prostate cancer. *Nat. Genet.* **39**, 954–956.
- Haiman, C.A., Patterson, N., Freedman, M.L., Myers, S.R., Pike, M.C., Waliszewska, A., Neubauer, J., Tandon, A., Schirmer, C., McDonald, G.J., et al. (2007b). Multiple regions within 8q24 independently affect risk for prostate cancer. *Nat. Genet.* **39**, 638–644.
- Hartmann, C., Meyer, J., Balss, J., Capper, D., Mueller, W., Christians, A., Felsberg, J., Wolter, M., Mawrin, C., Wick, W., et al. (2009). Type and frequency of IDH1 and IDH2 mutations are related to astrocytic and oligodendroglial differentiation and age: A study of 1,010 diffuse gliomas. *Acta Neuropathol.* **118**, 469–474.
- Hegi, M.E., Diserens, A.C., Gorlia, T., Hamou, M.F., de Tribolet, N., Weller, M., Kros, J.M., Hainfellner, J.A., Mason, W., Mariani, L., et al. (2005). MGMT gene silencing and benefit from temozolomide in glioblastoma. *N. Engl. J. Med.* **352**, 997–1003.
- Hegi, M.E., Liu, L., Herman, J.G., Stupp, R., Wick, W., Weller, M., Mehta, M.P., and Gilbert, M.R. (2008). Correlation of O6-methylguanine methyltransferase (MGMT) promoter methylation with clinical outcomes in glioblastoma and clinical strategies to modulate MGMT activity. *J. Clin. Oncol.* **26**, 4189–4199.
- Herman, J.G., and Baylin, S.B. (2003). Gene silencing in cancer in association with promoter hypermethylation. *N. Engl. J. Med.* **349**, 2042–2054.
- Hinoue, T., Weisenberger, D.J., Pan, F., Campan, M., Kim, M., Young, J., Whitehall, V.L., Leggett, B.A., and Laird, P.W. (2009). Analysis of the association between CIMP and BRAF in colorectal cancer by DNA methylation profiling. *PLoS ONE* **4**, e8357.
- Houshdaran, S., Hawley, S., Palmer, C., Campan, M., Olsen, M.N., Ventura, A.P., Knudsen, B.S., Drescher, C.W., Urban, N.D., Brown, P.O., and Laird, P.W. (2010). DNA methylation profiles of ovarian epithelial carcinoma tumors and cell lines. *PLoS ONE* **5**, e9359.
- Jones, P.A., and Baylin, S.B. (2007). The epigenomics of cancer. *Cell* **128**, 683–692.
- Kim, T.Y., Zhong, S., Fields, C.R., Kim, J.H., and Robertson, K.D. (2006). Epigenomic profiling reveals novel and frequent targets of aberrant DNA methylation-mediated silencing in malignant glioma. *Cancer Res.* **66**, 7490–7501.
- Kitarewan, S., Blumen, S., Sekula, D., Bissonnette, R.P., Lamph, W.W., Cui, Q., Gallagher, R., and Dmitrovsky, E. (2008). G0S2 is an all-trans-retinoic acid target gene. *Int. J. Oncol.* **33**, 397–404.
- Laird, P.W. (2003). The power and the promise of DNA methylation markers. *Nat. Rev. Cancer* **3**, 253–266.
- Liang, Y., Diehn, M., Watson, N., Bollen, A.W., Aldape, K.D., Nicholas, M.K., Lamborn, K.R., Berger, M.S., Botstein, D., Brown, P.O., and Israel, M.A. (2005). Gene expression profiling reveals molecularly and clinically distinct subtypes of glioblastoma multiforme. *Proc. Natl. Acad. Sci. USA* **102**, 5814–5819.
- Madhavan, S., Zenklusen, J.C., Kotliarov, Y., Sahni, H., Fine, H.A., and Buetow, K. (2009). Rembrandt: Helping personalized medicine become a reality through integrative translational research. *Mol. Cancer Res.* **7**, 157–167.
- Malik, M.A., Blusztajn, J.K., and Greenwood, C.E. (2000). Nutrients as trophic factors in neurons and the central nervous system: Role of retinoic acid. *J. Nutr. Biochem.* **11**, 2–13.
- Martinez, R., Schackert, G., and Esteller, M. (2007). Hypermethylation of the proapoptotic gene TMS1/ASC: Prognostic importance in glioblastoma multiforme. *J. Neurooncol.* **82**, 133–139.
- Martinez, R., Martin-Subero, J.I., Rohde, V., Kirsch, M., Alaminos, M., Fernandez, A.F., Roper, S., Schackert, G., and Esteller, M. (2009). A microarray-based DNA methylation study of glioblastoma multiforme. *Epigenetics* **4**, 255–264.
- Martinez, R., Rohde, V., and Schackert, G. (2010). Different molecular patterns in glioblastoma multiforme subtypes upon recurrence. *J. Neurooncol.* **96**, 321–329.
- Monti, S., Tamayo, P., Mesirov, J., and Golub, T. (2003). Consensus clustering: A resampling-based method for class discovery and visualization of gene expression microarray data. *Machine Learning* **52**, 91–118.
- Nagarajan, R.P., and Costello, J.F. (2009). Epigenetic mechanisms in glioblastoma multiforme. *Semin. Cancer Biol.* **19**, 188–197.
- Nakamura, M., Yonekawa, Y., Kleihues, P., and Ohgaki, H. (2001). Promoter hypermethylation of the RB1 gene in glioblastomas. *Lab. Invest.* **81**, 77–82.
- Ohgaki, H., and Kleihues, P. (2007). Genetic pathways to primary and secondary glioblastoma. *Am. J. Pathol.* **170**, 1445–1453.
- Parsons, D.W., Jones, S., Zhang, X., Lin, J.C., Leary, R.J., Angenendt, P., Mankoo, P., Carter, H., Siu, I.M., Gallia, G.L., et al. (2008). An integrated genomic analysis of human glioblastoma multiforme. *Science* **321**, 1807–1812.

- Phillips, H.S., Kharbanda, S., Chen, R., Forrester, W.F., Soriano, R.H., Wu, T.D., Misra, A., Nigro, J.M., Colman, H., Soroceanu, L., et al. (2006). Molecular subclasses of high-grade glioma predict prognosis, delineate a pattern of disease progression, and resemble stages in neurogenesis. *Cancer Cell* 9, 157–173.
- Pike, B.L., Greiner, T.C., Wang, X., Weisenburger, D.D., Hsu, Y.H., Renaud, G., Wolfsberg, T.G., Kim, M., Weisenberger, D.J., Siegmund, K.D., et al. (2008). DNA methylation profiles in diffuse large B-cell lymphoma and their relationship to gene expression status. *Leukemia* 22, 1035–1043.
- R Development Core Team (2009). R: A Language and Environment for Statistical Computing (Vienna: R Foundation for Statistical Computing).
- Sanson, M., Marie, Y., Paris, S., Idbaih, A., Laffaire, J., Ducray, F., El Hallani, S., Boisselier, B., Mokhtari, K., Hoang-Xuan, K., and Delattre, J.Y. (2009). Isocitrate dehydrogenase 1 codon 132 mutation is an important prognostic biomarker in gliomas. *J. Clin. Oncol.* 27, 4150–4154.
- Schumacher, F.R., Feigelson, H.S., Cox, D.G., Haiman, C.A., Albanes, D., Buring, J., Calle, E.E., Chanock, S.J., Colditz, G.A., Diver, W.R., et al. (2007). A common 8q24 variant in prostate and breast cancer from a large nested case-control study. *Cancer Res.* 67, 2951–2956.
- Shete, S., Hosking, F.J., Robertson, L.B., Dobbins, S.E., Sanson, M., Malmer, B., Simon, M., Marie, Y., Boisselier, B., Delattre, J.Y., et al. (2009). Genome-wide association study identifies five susceptibility loci for glioma. *Nat. Genet.* 41, 899–904.
- Silber, J.R., Blank, A., Bobola, M.S., Ghatan, S., Kolstoe, D.D., and Berger, M.S. (1999). O6-methylguanine-DNA methyltransferase-deficient phenotype in human gliomas: Frequency and time to tumor progression after alkylating agent-based chemotherapy. *Clin. Cancer Res.* 5, 807–814.
- Stone, A.R., Bobo, W., Brat, D.J., Devi, N.S., Van Meir, E.G., and Vertino, P.M. (2004). Aberrant methylation and down-regulation of TMS1/ASC in human glioblastoma. *Am. J. Pathol.* 165, 1151–1161.
- Sun, L., Hui, A.M., Su, Q., Vortmeyer, A., Kotliarov, Y., Pastorino, S., Passaniti, A., Menon, J., Walling, J., Bailey, R., et al. (2006). Neuronal and glioma-derived stem cell factor induces angiogenesis within the brain. *Cancer Cell* 9, 287–300.
- Tepel, M., Roerig, P., Wolter, M., Gutmann, D.H., Perry, A., Reifenberger, G., and Riemenschneider, M.J. (2008). Frequent promoter hypermethylation and transcriptional downregulation of the NDRG2 gene at 14q11.2 in primary glioblastoma. *Int. J. Cancer* 123, 2080–2086.
- Toyota, M., Ahuja, N., Ohe-Toyota, M., Herman, J.G., Baylin, S.B., and Issa, J.P. (1999). CpG island methylator phenotype in colorectal cancer. *Proc. Natl. Acad. Sci. USA* 96, 8681–8686.
- Uhlmann, K., Rohde, K., Zeller, C., Szymas, J., Vogel, S., Marczynek, K., Thiel, G., Nürnberg, P., and Laird, P.W. (2003). Distinct methylation profiles of glioma subtypes. *Int. J. Cancer* 106, 52–59.
- Vander Heiden, M.G., Cantley, L.C., and Thompson, C.B. (2009). Understanding the Warburg effect: The metabolic requirements of cell proliferation. *Science* 324, 1029–1033.
- Verhaak, R.G., Hoadley, K.A., Purdom, E., Wang, V., Qi, Y., Wilkerson, M.D., Miller, C.R., Ding, L., Golub, T., Mesirov, J.P., et al. (2010). Cancer Genome Atlas Research Network (2010). Integrated genomic analysis identifies clinically relevant subtypes of glioblastoma characterized by abnormalities in PDGFRA, IDH1, EGFR, and NF1. *Cancer Cell* 17, 98–110.
- Visakorpi, T., Kallioniemi, A.H., Syvänen, A.C., Hyytinen, E.R., Karhu, R., Tammela, T., Isola, J.J., and Kallioniemi, O.P. (1995). Genetic changes in primary and recurrent prostate cancer by comparative genomic hybridization. *Cancer Res.* 55, 342–347.
- Wajapeyee, N., Serra, R.W., Zhu, X., Mahalingam, M., and Green, M.R. (2008). Oncogenic BRAF induces senescence and apoptosis through pathways mediated by the secreted protein IGFBP7. *Cell* 132, 363–374.
- Weisenberger, D.J., Siegmund, K.D., Campan, M., Young, J., Long, T.I., Faasse, M.A., Kang, G.H., Widschwendter, M., Weener, D., Buchanan, D., et al. (2006). CpG island methylator phenotype underlies sporadic microsatellite instability and is tightly associated with BRAF mutation in colorectal cancer. *Nat. Genet.* 38, 787–793.
- Welch, C., Santra, M.K., El-Asaad, W., Zhu, X., Huber, W.E., Keys, R.A., Teodoro, J.G., and Green, M.R. (2009). Identification of a protein, G0S2, that lacks Bcl-2 homology domains and interacts with and antagonizes Bcl-2. *Cancer Res.* 69, 6782–6789.
- Yan, H., Parsons, D.W., Jin, G., McLendon, R., Rasheed, B.A., Yuan, W., Kos, I., Batinic-Haberle, I., Jones, S., Riggins, G.J., et al. (2009). IDH1 and IDH2 mutations in gliomas. *N. Engl. J. Med.* 360, 765–773.
- Yeager, M., Orr, N., Hayes, R.B., Jacobs, K.B., Kraft, P., Wacholder, S., Minichiello, M.J., Fearnhead, P., Yu, K., Chatterjee, N., et al. (2007). Genome-wide association study of prostate cancer identifies a second risk locus at 8q24. *Nat. Genet.* 39, 645–649.